J. Fluid Mech. (2006), *vol.* 549, *pp.* 61–69.
doi:10.1017/S0022112005007706 Printed in the United Kingdom

Pattern imaging of primary and secondary electrohydrodynamic instabilities

By FRANCISCO VEGA REYES[1,3] AND FRANCISCO J. GARCÍA[2,3]

[1]Department of Physics, Georgetown University, Washington, DC 20057, USA
fvega@physics.georgetown.edu

[2]Departamento de Física Aplicada I, EUITA, Universidad de Sevilla, Carretera de Utrera, km. 1, 41013 Sevilla, Spain

[3]Departamento de Electrónica y Electromagnetismo, Facultad de Física, Avda. Reina Mercedes s/n. 41012 Sevilla, Spain

(Received 17 June 2005 and in revised form 25 October 2005)

A little known electrohydrodynamic instability, which we call a rose window, is observed in air/liquid interfaces in electric fields with unipolar space charge distributions. Depending on the liquid properties, the rose window may appear from an initial rest state (primary instability) or on top of another instability, the classical unipolar-injection-induced instability, destroying its pattern (secondary instability). After imaging of the rose window, we use an edge-detection filter to find the instability threshold and study the characteristic pattern as a function of the liquid properties. Results show that the specific properties of the electric field, due to charge injection, are the cause of the rose-window and that the primary and secondary rose windows are essentially different instabilities.

1. Introduction

Controlling fluid interfaces through electric fields is of interest because of its possible industrial applications, for example in replicating microscale patterns, which can be used in electrostatic lithography (Schaffer *et al.* 2000). In deforming a fluid interface with an electric field, the study of electrohydrodynamic (EHD) instabilities is a starting point. Electrohydrodynamic instabilities in plane fluid interfaces have been extensively studied in the absence of space charge distributions (Taylor & McEwan 1965; Melcher & Taylor 1969). However, for a complete study in a more general frame, non-zero space charge distributions need to be considered. The appearance of non-zero electric field divergences fundamentally changes the nature of the EHD instability problem, giving rise to a new set of less known instabilities that can only be described through the appropriate new electric field solutions (Atten 1969; Lacroix, Atten & Hopfinger 1975).

Thus we focus in this work on the less known EHD instabilities produced by electric fields in the presence of a space charge source, in the even less known particular case of a fluid interface. In particular we study the long-wave instability patterns (cell size is always much larger than the liquid layer thickness) observed in air/low-conducting-liquid interfaces under corona discharge. The term rose window, due to the tendency to form hexagonal cells, has been used up to now for all these patterns with a long characteristic wavelength (Vega & Pérez 2003). Although the rose window has been known for a long time, knowledge of its main characteristics has remained scarce: it

was observed in a very preliminary experimental work by Herrick (1974), but in that work it was not differentiated from the other patterns (convective instabilities). In some low-conducting liquids the rose window is the first EHD instability to appear when the electric field is increased (primary instability). But there are also liquids where the first instability to appear is another one that is caused by electrostatic repulsion in the bulk of the liquid (Lacroix *et al.* 1975), which produces a convection (hence, the name 'convective instability'). This instability has been more extensively studied, and for this reason we refer to it as the 'classical EHD instability' produced by space charge injection. If the electric field is increased enough, the rose window appears on top of this instability (Vega & Pérez 2003) gradually substituting the original pattern by another one with a 10 times larger length scale (the rose window is now a secondary instability).

In Vega & Pérez (2003), it was suggested that the primary rose window occurred in liquids in the ohmic regime of conduction, while the secondary rose window appeared in the non-ohmic regime. Both cases were identified as the same instability. We show now with experimental evidence that the primary and secondary rose windows are actually different instabilities with peculiar properties and verify that they correspond respectively to ohmic and non-ohmic regimes in the liquids. The cause of the primary instability has been explained theoretically in a recent study (Vega & Pérez 2002), where the electric field corresponding to a non-ohmic/ohmic fluid interface in the presence of a space charge source is written for the first time, together with the set of hydrodynamic equations to Navier–Stokes order (Batchelor 1967; Agarwal, Yun & Balakrishnan 2001). The present work is the first systematic experimental study of the instabilities in a variety of liquids with different ranges of electric conductivities and viscosities. More generally, these are the first measurements in a wide range of various liquid properties of a space-charge-induced EHD instability of any kind.

Corona discharge (Sigmond 1978) is used in our experiments as a unipolar space charge source (the ions injected at the interface have the same polarity), although other experimental methods can be used (Koulova-Nenova, Atten & Malraison 1996). Due to the large differences between the viscosities of the liquids and the air, the gas flow produced by the corona does not generate liquid movement and is not coupled to the problem of our interest, the air/liquid interface instability due to the action of the electric field (Vega & Pérez 2002). We also implement for all sets of measurements a new automated technique for instability pattern imaging.

2. Experimental set-up

The experimental set-up (figure 1) consists of a tip-plane two-electrode configuration in the air, where the tip is connected to a high DC voltage source and is placed above the centre of a circular plane electrode (4.5 cm diameter) that is grounded (Vega & Pérez 2003). An adjustable quantity of liquid (see table 1 for details on liquid properties) is deposited on the plane electrode in each experiment. The typical liquid volume used in the experiments is of the order of 2 ml, equivalent to a liquid layer depth of the order of 1 mm, and is controlled with a precision of 0.01 ml. The tip-to-plane electrode distance (h) is controlled by a micrometer with a precision of 10 μm. The typical tip height values are of the order of 3 to 4 cm. The tip begins to produce ions when the corona onset voltage V_0 is reached (Sigmond 1978), which in our set-up occurs typically around 3.5 kV. These ions are injected into the air and driven by the electric field onto the fluid interface, which is eventually deformed if the applied voltage V is increased sufficiently.

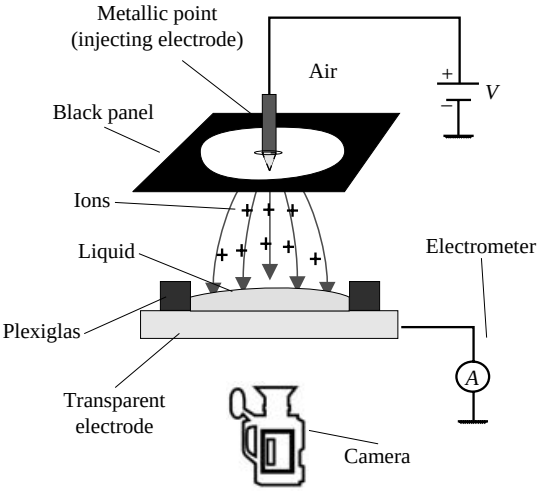

FIGURE 1. Experimental set-up.

	$\sigma\ (\Omega^{-1}\mathrm{m}^{-1})$	$\nu\ (\mathrm{cSt})$	$\varepsilon/\varepsilon_0$	$\gamma\ (\mathrm{mN\,m}^{-1})$	$\rho\ (\mathrm{g\,cm}^{-3})$
Silicone oil 50	1.3×10^{-13}	57.0	2.7	21.3	0.959
Silicone oil 1k	1.2×10^{-13}	984	2.8	21.4	0.971
Silicone oil 10k	1.8×10^{-13}	1.03×10^{4}	2.7	21.5	0.971
Isopar® L	1.7×10^{-12}	2.00	2.0	24.2	0.763
Isopar® L 10^{-5} M AOT	8.0×10^{-12}	2.00	2.0	24.2	0.763
Olive oil	1.2×10^{-11}	76.5	3.0	32.8	0.957
Castor oil	2.8×10^{-11}	702	4.4	37.4	0.916
Sunflower oil	6.4×10^{-11}	52.4	3.0		0.916
Corn oil	7.4×10^{-11}	56.4	3.0		0.916
Isopar® L 4×10^{-3} M AOT	1.0×10^{-10}	2.00	2.0	24.2	0.763
Isopar® L 4×10^{-2} M AOT	2.0×10^{-9}	2.00	2.0	24.2	0.763
Isopar® L 9.54×10^{-3} M AOT $+10^{-5}$ M Aloha	5.0×10^{-8}	2.00	2.0	24.2	0.763
Glycerin	3.9×10^{-6}	759	46	63.4	1.26
Water	2.6×10^{-2}	0.898	79	72.0	0.997

TABLE 1. Properties of the liquids used in the experiments: electric conductivity, viscosity, relative dielectric constant (to the dielectric constant of air), capillarity (air/liquid interface) and mass density, respectively. These properties were measured in our laboratory, at constant atmospheric pressure and a temperature of $25\pm2\,^{\circ}\mathrm{C}$. For varying only conductivity, we used solutions with different concentrations of di-2-ethylhexyl sodium sulfosuccinate (AOT) and bis(3,5-di-t-butylsalicylate) aluminum hydroxide (Aloha) in one of the liquids, Isopar® -L (Isoparaffin, C_nH_{2n+2}). For varying only viscosity we used different Rhodorsil® silicone oils, with three viscosities. This allows experiments to be performed with different conductivities or viscosities without changing other liquid properties like mass density.

The plane electrode, connected to an electrometer, is transparent (glass coated with a thin conducting film). This allows imaging of the air/liquid interface from below because all liquids used in the experiments are transparent. An analog video camera takes images and movies of the experiments. A horizontal black panel, placed above the plane, with an inner white circle (a sheet of white paper) is used to obscure the visual area falling outside the plane electrode (figure 1). A small hole in the centre of

the white circle allows the tip just to pass perpendicularly through it. A thin insulating tube covering the metallic point (except at the tip) prevents electrical contact with the paper. The system is lighted from above the panel. An image-acquisition board captures the images and saves them to a computer. The movies are saved to a video recorder. All experiments are automated by a second computer from which we control the applied electric voltage and to which we save the electric current measurement, averaged in stationary state at constant applied voltage from a set of readings. Each reading is performed during a small time interval (compared to the characteristic transient time).

3. Image processing

The human-eye-based determination of the voltage at which the instability begins has some shortcomings. First, the measure is based on a human decision on the minimum voltage for which the instability is apparent. Second, it cannot be implemented automatically. An alternative machine-based method is desirable for automatic implementation and validation of the first method.

We have implemented an image-processing method, based on *SUSAN* image filters (Smith & Brady 1997), that determines the minimum voltage for which the instability appears. First, we produce a voltage-increasing sequence of direct (unprocessed) images, from values for which there is no instability to values where it is clearly developed. For each image, our method computes the number of image pixels (N) at the optical edges characterized by having a local maximum of intensity gradient. The fluid interface is lighted and imaged in such a way that the instability cell edges in the unprocessed images appear as dark borders, due to the reflection of light rays coming from the curved fluid interface off the black panel, while the inner part of the instability cells remains white. In this way, the optical edges in the images coincide with the instability cell edges except for a constant number N_0 corresponding to the plane electrode edges and the small image of the tip in the centre. Thus, the number N is expected to equal the constant N_0 when the applied voltage is under the rose window critical value; at the critical voltage, interfacial perturbations develop, which leads to an increase in N. This first change in N indicates the instability threshold. When the rose window is secondary, the processing parameters can be chosen so that the measurement is not sensitive to the first instability, the classical unipolar-injection-induced electrohydrodynamic instability (Lacroix *et al.* 1975), due to the small size of its hexagonal cells (of the order of less than 1 mm) and weak interface deformation compared to the rose window's.

The steps of our image-processing technique are: filtering for diminishing noise (Russ 1999), edge-detection filtering, and thinning of the edges. These are presented in figure 2 for a typical image of the instabilities.†

4. Results

We observed in all measurements that above the rose-window threshold V_c and over a wide range of the applied voltage the total length of edges in the images increases monotonically. The intersection of a linear or parabolic fitting of $N(V)$ for $V > V_c$ with N_0 provides a measure of V_c. The total number of edge points N is

† More details of the image processing, and movies showing the development of the instability, are provided in an online supplement to this paper.

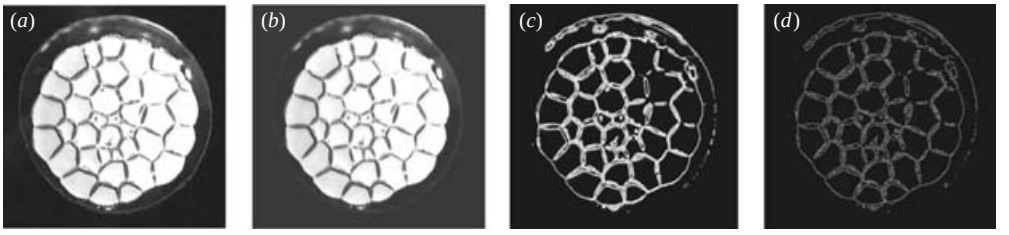

FIGURE 2. Image processing stages. (*a*) Original image. (*b*) After smoothing. (*c*) Edge-detector map. (*d*) After thinning edges.

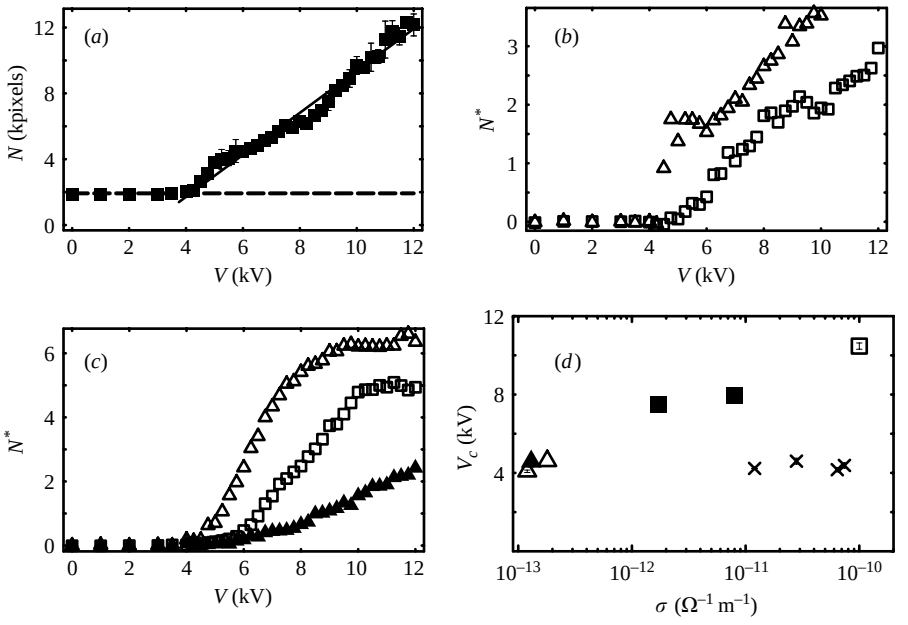

FIGURE 3. (*a*) N vs. applied voltage V. Sunflower (conductivity $\sigma = 6.4 \times 10^{-11}\,\Omega^{-1}\,\mathrm{m}^{-1}$, viscosity $\nu = 52.4$ cSt), Vol = 2.0 ml (equivalent to a 1.26 mm liquid layer thickness). Tip-to-plane distance $h = 4.0$ cm. The solid line is the linear fit and the dashed line is the base level N_0. (*b*) N^* vs. applied voltage V. Olive (△) and Corn oil (□). $\sigma = 1.2 \times 10^{-11}\Omega^{-1}\,\mathrm{m}^{-1}$ and $\sigma = 7.4 \times 10^{-11}\Omega^{-1}\,\mathrm{m}^{-1}$ respectively, $\nu \sim 60.0$ cSt, Vol = 2.0 ml, $h = 4.0$ cm. (*c*) Silicone oils ($\sigma \sim 10^{-13}\Omega^{-1}\,\mathrm{m}^{-1}$), different viscosities: 50 cSt (▲); 1000 cSt (△); and 10 000 cSt (□). Vol = 2.0 ml, $h = 4.0$ cm. (*d*) Critical values of the rose-window voltage vs. electric conductivity. Here, the different symbols indicate different groups of liquids: triangles silicone oil and squares Isopar® -L while crosses indicate oils (primary instability) with other varying properties: olive, castor, sunflower and corn oil, from left to right. Vol = 2.0 ml, $h = 4.0$ cm. In (*b*), (*c*) and (*d*) open and solid symbols denote primary and secondary instability respectively.

plotted against the applied voltage in figure 3(*a*). The error bars show the typical reproducibility of our measurement of $N(V)$.

Concerning the distinction between primary and secondary long-wave instabilities (the rose windows), Vega & Pérez (2003) suggested that the origin of the absence of the classical EHD instability in certain low-conducting liquids could be due to a transition in the electric conduction regime, from non-ohmic to ohmic. This was based on the fact that the classical EHD instability necessarily occurs in a liquid in the non-ohmic regime of electric conduction (Lacroix *et al.* 1975). Thus, the

	$K(\mathrm{m^2\,V^{-1}\,s^{-1}})$	C_0	rose-window type
Silicone oil 50	5.0×10^{-10}	0.11	Secondary
Silicone oil 1k	2.5×10^{-11}	1.70	Primary
Silicone oil 10k	2.5×10^{-12}	27.43	Primary
Isopar® L	2.4×10^{-8}	0.11	Secondary
Isopar® L 10^{-5} M AOT	2.4×10^{-8}	0.29	Secondary
Castor oil	4.0×10^{-11}	178.1	Primary
Corn oil	4.5×10^{-10}	611.2	Primary
Isopar® L 4×10^{-3} M AOT	2.4×10^{-8}	3.68	Primary
Isopar® L 4×10^{-2} M AOT	2.4×10^{-8}	73.56	Not observed
Isopar® L 9.54×10^{-3} M AOT 10^{-5} M Aloha	5.0×10^{-8}	$\gg 1$	Not observed
Glycerin	—	$\gg 1$	Not observed
Water	—	$\gg 1$	Not observed

TABLE 2. Observed type of rose window in the liquids, for different values of C_0. V_l is estimated from the expressions for the electric field in a non-ohmic/non-ohmic interface under injection, in plane geometry for the liquid layer thickness corresponding to a volume of 2 ml in the experiments, and $h = 4.0$ cm. The last column gives the experimentally observed rose-window instability type and agrees, as we see, with the type predicted from the value of C_0.

secondary-to-primary rose-window transition was described with the help of the parameter $C_0 = d^2\sigma/(K V_l \varepsilon)$, where K is the fluid ion mobility and V_l is the electric potential drop through a liquid layer with thickness d. This parameter allows us to predict the electric conduction regime in the liquid, giving a non-ohmic conduction regime in the liquid for $C_0 < 1$ and therefore a secondary rose-window instability and an ohmic conduction regime for $C_0 > 1$ (primary rose window). Briefly, this is so because C_0 is a relationship between the non-ohmic conduction characteristic time $\tau_{no} = d^2/(K V_l)$ and the ohmic relaxation time $\tau_o = \varepsilon/\sigma$: if $\tau_{no} < \tau_o$ (i.e. $C_0 < 1$), then the charges are conducted through the liquid before they relax and the conduction is non-ohmic and vice versa for $\tau_{no} > \tau_o$ ($C_0 > 1$). Our experimental observations agree with this description, as can be seen in table 2, where we present the rose-window type observed in the liquids, compared to the value of C_0 (Vega & Pérez 2003). Therefore, it is justified to identify the primary and secondary instability in low-conducting liquids with ohmic and non-ohmic regime respectively, and we will also use those terms from now on.

$N^* = N/N_0 - 1$ is plotted against the applied voltage for liquids with different conductivities and similar viscosities in figure 3(b) and vice versa in figure 3(c). Usually, $N^*(V)$ is a smoothly increasing function for $V > V_c$, but in the curve for olive oil it has a finite jump (figure 3b). This happens if the actual value of the critical voltage $V_c < V_0$ (being V_0 the corona onset voltage): in this case there is no charge injection at V_c and consequently the instability cannot develop below V_0. Once V_0 is reached, the interface begins to receive charge injection at a voltage higher than V_c and therefore the instability appears abruptly.

In the increasing $N^*(V)$ regime, and for non-ohmic and viscous ohmic liquids, the instability cells tend to acquire steady polygonal forms like hexagons or pentagons and their typical size decreases when the voltage is increased, with this decreasing tendency much stronger in the ohmic case. After that, a new regime is reached where the effect of increasing the voltage is to break the cells polygonal regularity (ohmic viscous liquids) and/or to break the cells steadiness (all liquids), rather than to decrease their size (figure 4). Eventually, in this regime and for ohmic viscous

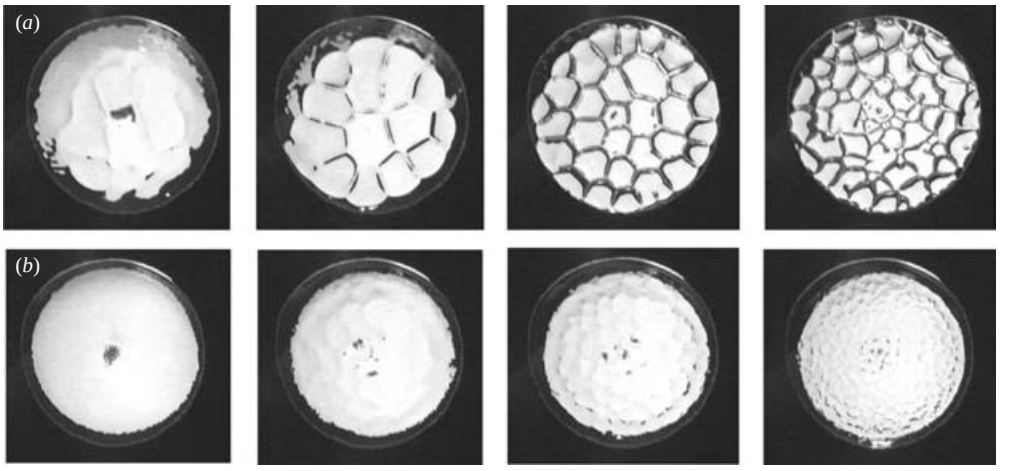

FIGURE 4. Unprocessed images of the interface patterns. (*a*) Ohmic liquid (silicone oil (1000 cSt), primary instability). From left to right, voltages: 4.75 kV; 5.5 kV; 7.25 kV; 10.0 kV. Vol = 2.0 ml, $h = 4.0$ cm. (*b*) Non-ohmic liquid (silicone oil (50 cSt, secondary instability). From left to right, voltages: 5.5 kV (only the smaller pattern of the bulk instability is observed in this image); 7.25 kV (rose window is already present); 9.5 kV; 14 kV. Vol = 1.5 ml, $h = 4.0$ cm.

liquids, $N^*(V)$ saturates and tends to remain constant (figure 3*c*), in the range of our observations. In ohmic liquids with lower viscosities, the instability cells, from the instability onset, tend to form more irregular structures (see also the movies in the online supplementary material), whose steadiness disappears rapidly as the voltage is increased.

We found that in the Isopar®-L solutions, whose only varying property is the conductivity, V_c increases with conductivity in non-ohmic and ohmic regimes (figure 3*d*). The increase of V_c in the non-ohmic case is due to the different values taken by the injected space charge through the fluid interface for different conductivity values (Denat 1982) (it is known that (Lacroix *et al.* 1975; Vega & Pérez 2002) the injection level $C = q_0 h^2/\varepsilon_0 V$ is an essential control parameter in the space-charge-induced instabilities, where q_0 is the space charge at the injecting electrode, the metallic tip in our case, and h a characteristic length in the system). For the group of liquids with different varying properties (corn, castor, olive and sunflower oils), it was not possible to find a well-defined trend as a function of conductivity, which is evidence of the importance of other properties, like dielectric permittivity, following a previous theoretical analysis (Vega, Pérez & Castellanos 2003). However, the influence of viscosity in the rose-window instability threshold is much less important than the influence of conductivity (compare silicone oil and Isopar®-L series in figure 3*d*).

Another novel observation is the transition from a primary to secondary rose window by varying the conductivity (Isopar®-L series) or the viscosity (silicone oil series) and keeping the other liquid properties constant (figure 3*c*, *d*). This observation has the additional value of also involving the classical EHD instability (it is, to our knowledge, the first observation of its disappearance by varying only one liquid property). We also observed a remarkable difference between the threshold characteristic wavelength in the primary and secondary rose windows (figure 4): while in the primary instability it is infinite (the deformation does not form any closed cells), it is finite in the secondary instability (the instability first appears in the form of polygonal cells). It is also to be noticed in figure 4 that the interface deformation

is much stronger in the ohmic case. This is also reflected in the fact that the cell edges in the processed images are better defined for the ohmic case. Furthermore, there is a significatively steep increase in the average value of $N^*(V)$ when a transition from secondary to primary instability is observed if the viscosity is raised (figure 3*c*). After this transition, N^* decreases if the viscosity continues to be increased (figure 3*c*). Taking into account these observations (very different critical wavenumber and $N^*(V)$ curves) and their very different dynamics (see the movies in the online supplementary material), we may conclude that primary and secondary rose windows correspond to very different instabilities.

5. Conclusion

With our image processing method we can track quantitatively interface deformation, which allows us to detect the instability thresholds and to characterize the instability patterns. The experimental method has also the following advantages: no additive substances in the liquid, which change its properties, are needed; it can be used in other fluid dynamics problems; and, in future research, additional processing of the images, like Fourier transform spectra representation, may eventually lead to obtaining systematically more information on the geometrical characteristics or dynamical behaviour of the patterns (Egolf, Melnikov & Bodenschatz 1998).

As a general conclusion, a lack of uniformity has been found, in the different liquids, in the observed patterns and dynamics of what had been previously characterized as a single phenomenon called rose window instability (this is reflected in the $N^*(V)$ curves, for instance). Furthermore, the systematic use of a variety of liquids with a widely varying range of properties has allowed us: (*a*) to detect new and previously unclassified patterns (for example, the irregular characteristic pattern in ohmic liquids with low viscosities and its rapid transition to chaotic dynamics, see the online supplementary material); and (*b*) to distinguish experimentally the different origins of the primary and secondary instabilities. Moreover, good agreement is found between the experimentally observed type of long-wave instability (primary/secondary) and the theoretically predicted type, using the value of the parameter C_0 (table 2). Thus, a general and rational classification follows, including for the first time all types of space-charge-induced instabilities observed in our system: (i) the classic EHD instability in low-conducting liquids, a hexagonal pattern with a short wavelength, is only observed when the charge relaxation time is sufficiently long compared to the non-ohmic conduction characteristic time ($C_0 < 1$; i.e. non-ohmic regime); (ii) after this instability and in the non-ohmic regime a secondary instability appears, characterized by a (finite) long wavelength, a regular hexagonal pattern and a slight interface deformation; (iii) this is in contrast to the long-wave instability observed in liquids in the ohmic regime (with $C_0 > 1$), which is primary and first appears with an infinite wavelength, a very strong and static interface deformation and an irregular pattern. All this leads us to consider the secondary rose window in the non-ohmic regime to be a convective instability, caused by a bifurcation in the characteristic wavelength of the classic EHD instability. On the contrary, the observations reveal that the primary long-wave instability in the ohmic regime is a different instability, with a static interfacial deformation; more importantly, its tendency to disappear at high conductivities is in agreement with previous theory (Vega & Pérez 2002).

Hence, the results in this work are the first systematic experimental evidence of the new electric field solution described in a previous work (Vega & Pérez 2002) and work in preparation. They also provide further evidence of the original behaviour of

a system with an electric field solution due to the presence of space charge sources (Atten 1969; Lacroix *et al.* 1975). This type of electrostatic field solution is perhaps not in general as widely known as those without space charge sources. The possible practical applications of this type of electric field still remain in many cases an open issue.

The authors thank A. Castellanos for valuable comments. This work was supported by the Spanish Ministry of Science and Technology under research project BFM-2003-01739. F.V.R. is also supported by the Spanish Government as an FPI-MECD and SEEU Fellow (Secretariat of State of Education and Universities, ref. GT2002-0023).

REFERENCES

Agarwal, R. K., Yun, K. & Balakrishnan, R. 2001 *Phys. Fluids* **13**, 3061.

Atten, P. 1969 Étude mathématique du problème du champ électrique affecté par un flux permanent d'ions unipolaires et application à la théorie de la sonde froide. PhD thesis, Université de Grenoble, France.

Batchelor, G. K. 1967 *An Introduction to Fluid Dynamics*. Cambridge University Press.

Denat, A. 1982 Étude de la conduction électrique dons les solvants non polaires. PhD thesis, Université de Grenoble, France.

Egolf, D. A., Melnikov, I. V. & Bodenschatz, E. 1998 *Phys. Rev. Lett.* **80**, 3228.

Herrick, C. S. 1974 *Proc. R. Soc. Lond.* A **336**, 487.

Koulova-Nenova, D., Atten, P. & Malraison, B. 1996 In *Conference Record of the 12th International Conference on Dielectric Liquids (ICDL 96, Rome, Italy)*, p. 472.

Lacroix, J. C., Atten, P. & Hopfinger, E. J. 1975 *J. Fluid Mech* **69**, 539.

Melcher, J. R. & Taylor, G. I. 1969 *Annu. Rev. Fluid Mech.* **1**, 111.

Russ, J. C. 1999 *The Image Processing Handbook*, 3rd edn. CRC Press–IEEE Press, Boca Raton, FL.

Schaffer, E., Thurn-Albrecht, T., Russell, T. P. & Steiner, U. 2000 *Nature* **403**, 874.

Sigmond, R. S. 1978 Corona discharges. In *Electrical Breakdown of Gases*. (ed. J. M. Meek & J. D. Craags). Wiley.

Smith, S. & Brady, J. 1997 *Intl J. Computer Vision* **23**, 45.

Taylor, G. I. & McEwan, A. 1965 *J. Fluid Mech.* **22**, 1.

Vega, F. & Pérez, A. T. 2002 *Phys. Fluids* **14**, 2738.

Vega, F. & Pérez, A. T. 2003 *Exps. Fluids* **34**, 726.

Vega, F., Pérez, A. T. & Castellanos, A. 2003 In *Annual Report of the Conference on Electrical Insulation and Dielectric Phenomena (CEIDP)*, p. 674.